

# The Sensitivity of Low Flip Angle RARE Imaging

David C. Alsop

**It is demonstrated that the stability of the Carr-Purcell-Meiboom-Gill (CPMG) sequence reflects the existence of a steady state solution to the Bloch equations in the absence of  $T_2$  and  $T_1$  decay. The steady state theory is then used to evaluate the performance of low flip angle RARE imaging sequences with both constant and optimally varied refocusing flip angles. The theory is experimentally verified in phantoms and then optimized, single shot, low flip angle RARE is used to obtain artifact-free images from the brain of a normal volunteer.**

**Key words:** RARE; fast imaging; magnetic resonance imaging.

## INTRODUCTION

RARE imaging (1) is a method to increase the speed of spin-echo imaging by acquiring a series of spin echoes with different phase encodings after each excitation. Because the technique offers either shorter scan times or higher signal-to-noise ratio than standard spin-echo imaging while producing similar contrast (2, 3), RARE imaging has become a clinical success. The faster speed of RARE imaging has allowed increased flexibility in choosing  $TR$  for optimal contrast and has improved the feasibility of inversion recovery preparation (4). In clinical applications, usually fewer than 16 echoes are employed, although in specialized applications where long  $T_2$  fluid is being imaged, such as MR cholangiography (5), longer echo trains are feasible.

It is straightforward to further increase the speed of RARE imaging by acquiring a larger number of spin echoes but this approach eventually leads to several problems. One major concern is RF power deposition within the subject. A long series of compact  $180^\circ$  pulses can readily introduce more RF heating than is acceptable according to normal safety guidelines, particularly if multiple slices are being acquired. A long train of  $180^\circ$  pulses also increases the interaction between neighboring slices and can lead to undesirable loss of contrast and signal. At the power levels employed in long echo train RARE imaging, magnetization transfer saturation (6) is quite significant and can increase the effective slice interaction. Finally, unless all the echoes are acquired within a time on the order of  $T_2$ , significant distortion of the point spread function of the image will occur (1, 7, 8). This requirement places a strong restriction on the length of an echo train.

---

MRM 37:176-184 (1997)

From the Department of Radiology, University of Pennsylvania Medical Center, Philadelphia, Pennsylvania.

Address correspondence to: David Alsop, Ph.D., Department of Radiology, University of Pennsylvania Medical Center, 3400 Spruce Street, Philadelphia, PA 19104-4283.

Received July 16, 1996; revised September 24, 1996; accepted September 26, 1996.

This research was supported in part by a Biomedical Engineering Research Grant from the Whitaker Foundation.

0740-3194/97 \$3.00

Copyright © 1997 by Williams & Wilkins

All rights of reproduction in any form reserved.

These limitations of RARE imaging were recognized by one of its inventors (9) and the use of reduced flip angles for the refocusing pulses was proposed as a solution. When these reduced flip angle pulses are used, the echo amplitude becomes a complex combination of stimulated echoes and spin echoes. It was demonstrated with numerical simulations and experiments in long  $T_2$  specimens that the spin echo amplitude approaches a temporary steady state which then slowly decays due to  $T_2$  and  $T_1$  relaxation. Because the "steady state" is actually only temporary, it will be referred to as a pseudosteady state. The empirically determined pseudosteady state echo amplitude was well approximated by the sine of half the refocusing flip angle. The use of a reduced flip angle dramatically decreases the power deposited by the sequence and also reduces the slice interaction.

A method for optimizing the flip angles of the first few refocusing pulses to achieve a constant amplitude echo train was later presented by LeRoux and Hinks (10). They demonstrated that beginning the RF pulse train with higher amplitude pulses that slowly decrease and approach a constant, or asymptotic, flip angle can produce a constant echo amplitude from the very first echo. Although this work was primarily focused on stabilizing the signal when large flip angle, slice selective pulses were employed, the approach also eliminated the primary drawback of constant flip angle, low flip angle RARE: the large number of echoes which have to be discarded until the pseudosteady state is reached. In addition, the optimized flip angle approach produced pseudosteady state echo amplitudes that were considerably higher than when a corresponding constant flip angle RF train was employed.

The dependence of the pseudosteady state echo amplitude on the flip angles of the early pulses in the RF pulse train raises two questions whose answers will determine the quality and utility of low flip angle RARE imaging: What is the highest pseudosteady state echo amplitude attainable for a given asymptotic flip angle and what RF pulse trains can achieve this amplitude? Below an analytical solution for the pseudosteady state spin echo train is derived that provides an upper limit for the attainable pseudosteady state echo amplitude. The solution is then employed to assess the efficiency of different RF pulse trains for producing magnetization in the pseudosteady state condition and to evaluate the utility of low flip angle RARE imaging. Finally the conclusions are evaluated experimentally in both phantoms and a normal volunteer.

## THEORY

### Pseudosteady State Solution

A steady state solution to the Bloch equation has been derived for the short  $TR$  gradient echo sequence by following the evolution of the magnetization from one ex-

citation to the next and requiring that the net change is zero (11). A similar method will be used below for the spin echo pseudosteady state. Because the spin echo pseudosteady state is not stable against  $T_1$  and  $T_2$  decay, terms involving  $T_1$ ,  $T_2$  and consequently  $M_0$  in the Bloch equations will be ignored. Because RF pulses cause only rotation, the effect of the RF pulse can be expressed in terms of three Euler angles: a rotation around the  $z$  axis of angle  $\beta$  followed by a rotation around the  $y$  axis of angle  $\alpha$ , and finally a rotation around the  $z$  axis of angle  $\delta$ . This can be written in matrix form (12) as

$$\begin{pmatrix} M'_t \\ M^{*\prime}_t \\ M'_z \end{pmatrix} = \begin{pmatrix} \cos^2 \frac{\alpha}{2} \exp i(\beta + \delta) & -\sin^2 \frac{\alpha}{2} \exp -i(\beta - \delta) & -\sin \alpha \exp i\delta \\ -\sin^2 \frac{\alpha}{2} \exp i(\beta - \delta) & \cos^2 \frac{\alpha}{2} \exp -i(\beta + \delta) & -\sin \alpha \exp -i\delta \\ \frac{\sin \alpha}{2} \exp i\beta & \frac{\sin \alpha}{2} \exp -i\beta & \cos \alpha \end{pmatrix} \cdot \begin{pmatrix} M_t \\ M^{*\prime}_t \\ M_z \end{pmatrix} \quad [1]$$

where  $M_t$  is the complex transverse magnetization given by

$$M_t = M_x + iM_y \quad [2]$$

Define the magnetization as equal to  $M^1$  at echo 1. The magnetization experiences a phase rotation of  $\phi/2$  followed by the RF pulse and a second rotation of  $\phi/2$  before echo 2. The phase rotation,  $\phi$ , is caused by applied slice select and readout gradients as well as frequency offset from the transmitter frequency. This can be written as

$$\begin{pmatrix} M^2_t \\ M^{*\prime 2}_t \\ M^2_z \end{pmatrix} = \begin{pmatrix} \cos^2 \frac{\alpha}{2} \exp i(\beta + \delta + \phi) & -\sin^2 \frac{\alpha}{2} \exp -i(\beta - \delta) & -\sin \alpha \exp i\left(\delta + \frac{\phi}{2}\right) \\ -\sin^2 \frac{\alpha}{2} \exp i(\beta - \delta) & \cos^2 \frac{\alpha}{2} \exp -i(\beta + \delta + \phi) & -\sin \alpha \exp -i\left(\delta + \frac{\phi}{2}\right) \\ \frac{\sin \alpha}{2} \exp i\left(\beta + \frac{\phi}{2}\right) & \frac{\sin \alpha}{2} \exp -i\left(\beta + \frac{\phi}{2}\right) & \cos \alpha \end{pmatrix} \cdot \begin{pmatrix} M^1_t \\ M^{*\prime 1}_t \\ M^1_z \end{pmatrix} \quad [3]$$

The steady state requirement demands that  $M^2$  is equal to  $M^1$ . This system of equations can be solved directly, see Appendix, to yield

$$M^{*\prime}_t = -\exp i(\beta - \delta)M_t \quad [4]$$

$$M_z = \frac{i \sin \alpha \exp i\left(\frac{\beta - \delta}{2}\right) \sin \left(\frac{\beta + \delta + \phi}{2}\right)}{(1 - \cos \alpha)} M_t \quad [5]$$

Equation [4] determines the phase of the echo as a function of the phase of the RF pulse and is a statement of the Meiboom-Gill condition (13) for the stability of a spin echo train. Equation [5] determines the fraction of the magnetization along the longitudinal direction. If one assumes that all of the equilibrium magnetization,  $M_0$ , has been placed in the pseudosteady state condition, then the transverse magnetization is given by, see Appendix,

$$M_t = \pm i M_0 \exp -i\left(\frac{\beta - \delta}{2}\right) \cdot \left(1 + \frac{\left(\sin \alpha \sin \left(\frac{\beta + \delta + \phi}{2}\right)\right)^2}{(1 - \cos \alpha)}\right)^{-\frac{1}{2}} \quad [6]$$

The echo amplitude is given by averaging this expression over  $\phi$ . This average can be easily performed numerically but by making use of special functions and integral tables (14), one can also find an analytical solution, see Appendix,

$$M_{\text{echo}} = \pm i M_0 \exp -i\left(\frac{\beta - \delta}{2}\right) \left(\sin \frac{\alpha}{2}\right)^{\frac{1}{2}} P^{-\frac{1}{2}} \left(\sin \frac{\alpha}{2} \left(1 + \frac{1 \sin^2 \alpha}{8 \sin^4 \frac{\alpha}{2}}\right)\right) \quad [7]$$

where  $P$  is a Legendre function.

In Fig. 1, the theoretical pseudosteady state function, Eq. [7], is compared with the empirical formula for the amplitude when a constant flip angle RF pulse train is employed (9). The theoretical echo amplitude is larger than the constant flip angle echo amplitude for all flip angles. This discrepancy arises from the major unjustified assumption in the theoretical derivation: that all of the equilibrium longitudinal magnetization is transferred to the pseudosteady state. There is an inefficient transition to the pseudosteady state when a constant flip angle RF pulse train is used. It is possible to derive the echo amplitude produced by a constant flip angle RF pulse train by assuming that all magnetization not initially aligned with the pseudosteady state condition eventually dissipates. The  $90^\circ$  excitation pulse produces a purely transverse magnetization. Assuming the phase of the excitation pulse is chosen to satisfy the Meiboom-Gill condition (13), Eq. [4], the component of the excited magnetization along the pseudosteady state solution is determined by the angle between the pseudosteady state solution,  $M^{ss}$ , and the transverse plane.

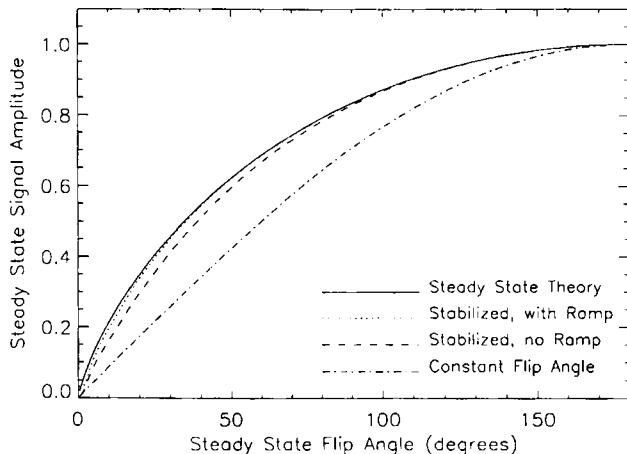


FIG. 1. Pseudosteady state RARE echo amplitudes as a function of the asymptotic refocusing flip angle. The theoretical pseudosteady state amplitude, solid line, represents the maximum possible amplitude achievable. The asymptotic echo amplitudes for a constant flip angle RF pulse train, a train optimized for constant echo amplitude, and one optimized for a short downward ramp in echo amplitude followed by constant echo amplitude are also plotted. The optimized RF pulse trains come closest to producing the optimal echo amplitude.

$$|M_t^{\text{const}}| = M_0 \frac{M_t^{\text{ss}}}{\sqrt{(M_t^{\text{ss}})^2 + (M_z^{\text{ss}})^2}} \quad [8]$$

$$\left( 1 + \left( \frac{\sin \alpha \sin \left( \frac{\beta + \delta + \phi}{2} \right)}{1 - \cos \alpha} \right)^2 \right)^{-\frac{1}{2}}$$

$$= M_0 \left( 1 + \left( \frac{\sin \alpha \sin \left( \frac{\beta + \delta + \phi}{2} \right)}{1 - \cos \alpha} \right)^2 \right)^{-1}$$

The average of this complex expression over all  $\phi$  is simply given by (14)

$$|M_{\text{echo}}^{\text{const}}| = M_0 \left( \sin \frac{\alpha}{2} \right) \quad [9]$$

in agreement with the earlier empirical result (9).

### Optimization of Echo Amplitudes

In the previous paragraph it was shown that the inefficiency of the constant flip angle RF pulse train reflects the difference in angular orientation of spins in the pseudosteady state condition compared with the spins placed in the transverse plane by the excitation pulse. One way to improve this efficiency is to slowly lower the flip angle of the RF pulse train from  $180^\circ$ , for which the pseudosteady state solution is in the transverse plane, to the desired asymptotic angle so the difference between the angle of the actual spins and the pseudosteady state solution is minimized. Because the flip angles used at the beginning of the echo train also have an impact on variations in the spin echo amplitude from echo to echo, it is

best to consider optimization of efficiency and stabilization of the echo amplitude simultaneously.

The method of Hennig (9) for calculating the echo amplitudes of an arbitrary RF pulse train was implemented. Following LeRoux and Hinks (10), the method was modified so that the flip angle of each subsequent RF pulse could be determined by specification of the desired amplitude of the echo produced by the pulse. To make possible the specification of other than constant echo amplitudes, an iterative determination of the flip angle was used in place of the exact solution developed by LeRoux and Hinks for the constant echo amplitude case. Beginning with the first echo, an initial guess for the flip angle was chosen. The amplitude of the echo was determined and then the guess for the flip angle was revised based on an iterative root finding algorithm. For simplicity only nonselective pulses were considered in the calculations. Figure 1 summarizes the results of the calculations. The theoretical pseudosteady state solution provides an upper bound to the attainable efficiency. The constant flip angle approach is clearly less efficient, especially at low flip angles. Amplitude stabilized echo trains, on the other hand, are highly efficient. An RF pulse train designed to produce a constant echo amplitude generates a signal very close to the optimal value at moderate to high asymptotic flip angles but the efficiency starts to drop at low asymptotic flip angles. The relatively high efficiency of the amplitude stabilized train can be attributed to the gradual decrease of the flip angle from angles near  $180^\circ$  at the first echo to the lower, constant flip angle used at large echo numbers. An example of an optimized RF pulse train is plotted in Fig. 2.

Intuitively, one would expect that increasing the flip angle of the first few RF pulses would further improve the efficiency of the echo train because the transition from transverse to pseudosteady state angles would be even more gradual. This can be achieved by specifying larger echo amplitudes for the first few echoes. RF pulse

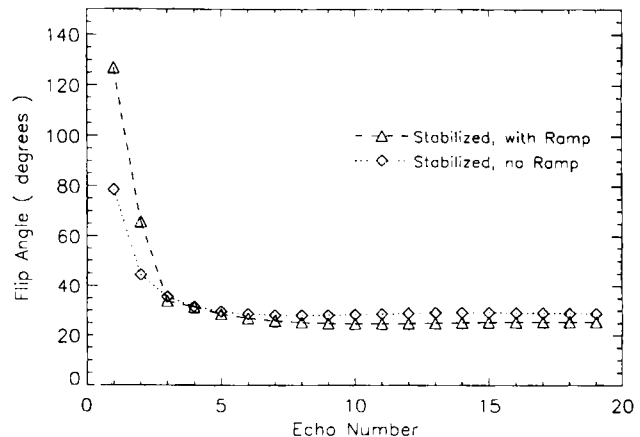


FIG. 2. Examples of echo amplitude stabilized RF pulse trains designed to achieve amplitudes of  $0.4 M_0$ . The constant echo amplitude RF pulse train, open squares, is slightly less efficient than the RF pulse train designed for an initial downward ramp in echo amplitude, open triangles, so a slightly larger asymptotic flip angle is required to achieve the same echo amplitude. Because of the initial downward ramp in echo amplitude, the ramp stabilized RF pulse train begins with a larger flip angle.

trains were therefore also calculated to produce a linear decrease in signal amplitude from echo one to echo three and an echo amplitude equal to the third echo amplitude for subsequent echoes. The slope of this amplitude ramp was chosen such that the amplitude of echo zero, if it existed, would be  $M_0$ . An example of such a ramp optimized RF pulse train is plotted in Fig. 2. The pseudosteady state echo amplitude achieved with this optimization approach is also plotted in Fig. 1 but it is so nearly identical to the theoretical optimum that it is partially obscured. Ramp optimized RF pulse trains are more efficient than constant optimized RF pulse trains but the higher echo amplitudes of the first two echoes must be magnitude corrected prior to image reconstruction.

### Effects of $T_2$ and $T_1$ Decay

The echo trains produced with multiple spin echoes are not truly in a steady state because  $T_1$  and  $T_2$  ultimately cause the decay of the signal. For perfect  $180^\circ$  pulses, only  $T_2$  affects the amplitude but when lower flip angles are used,  $T_1$  decay also plays a role because stimulated echoes are present. Once an RF pulse train has been selected, it is straightforward to insert  $T_1$  and  $T_2$  decay into the calculation of echo amplitudes. The echo amplitudes of the resulting echo trains do not decay as a perfect exponential. The effective  $T_2$  for the decay,  $T_{2\text{eff}}$ , was therefore defined as

$$T_{2\text{eff}}(T_2, T_1, \alpha) = \frac{2}{S(0, T_2, T_1, \alpha)^2} \int_0^\infty dt S(t, T_2, T_1, \alpha)^2 \quad [10]$$

where  $S(t, T_2, T_1, \alpha)$  is the echo amplitude as a function of time,  $T_2$ ,  $T_1$  and the refocusing flip angle,  $\alpha$ . This definition for  $T_{2\text{eff}}$  was chosen as the most appropriate for the discussion of signal-to-noise ratio which follows, and also yields the correct relaxation rate for an exponential decay. In Fig. 3, the ratio of  $T_{2\text{eff}}$  to  $T_2$  is plotted versus the ratio of  $T_1$  to  $T_2$  for several constant optimized RF pulse trains with different asymptotic flip angles. When  $T_1$  is long compared with  $T_2$ ,  $T_{2\text{eff}}$  is longer than  $T_2$

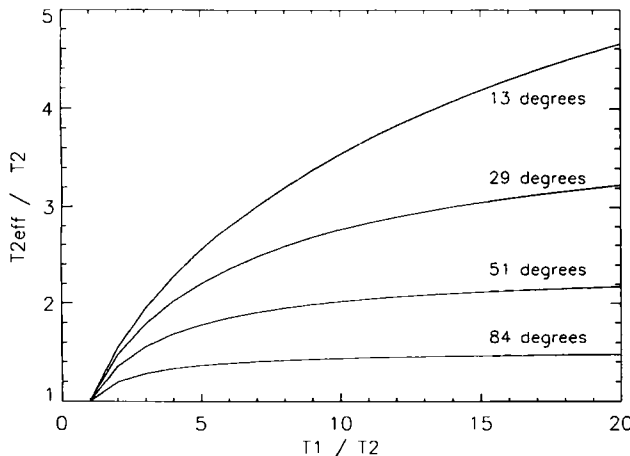


FIG. 3. The decay rate of the echo amplitudes,  $T_{2\text{eff}}$ , is plotted versus the ratio of  $T_1$  to  $T_2$  for several RF pulse trains with different asymptotic flip angles. The  $T_{2\text{eff}}$  was calculated from simulations of constant echo amplitude optimized RF pulse trains.

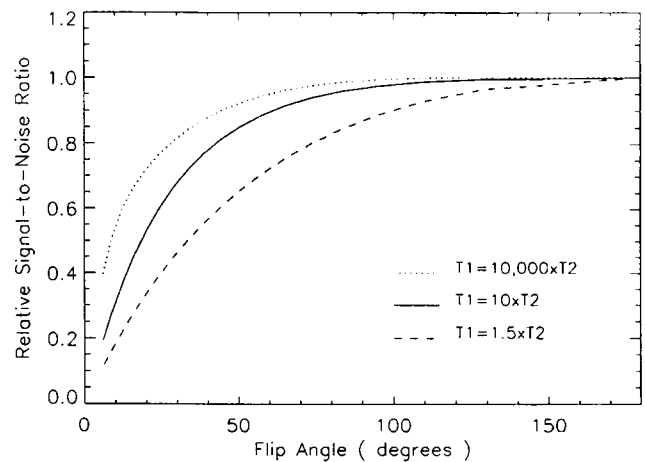


FIG. 4. The calculated signal-to-noise ratio versus asymptotic flip angle calculated by using Eq. [11] and the  $T_{2\text{eff}}$ 's plotted in Fig. 3. Signal-to-noise ratio decreases only very slowly with the refocusing flip angle.

but still relatively independent of  $T_1$  except at very small asymptotic flip angles. When  $T_1$  becomes comparable with  $T_2$ , the contribution of  $T_1$  to  $T_{2\text{eff}}$  is considerable.

### Signal-to-Noise Ratio of Low Flip Angle RARE

Although the use of lower flip angles in RARE imaging necessarily reduces the acquired echo amplitude, the signal-to-noise ratio need not decrease proportionately. Because the  $T_{2\text{eff}}$  of low flip angle RARE is longer than that of  $T_2$ , there is more time to acquire signal. Consequently, signal averaging of echoes or, alternatively, narrower bandwidth acquisitions can be used to reduce the measured noise. Employing the matched filter approach of Ernst and Anderson (11), the relative signal-to-noise ratio of low flip angle RARE is given by

$$\text{SNR}_{\text{rel}} = \frac{S(0, T_2, T_1, \alpha)}{S(0, T_2, T_1, 180)} \left( \frac{T_{2\text{eff}}(T_2, T_1, \alpha)}{T_{2\text{eff}}(T_2, T_1, 180)} \right)^{\frac{1}{2}} \quad [11]$$

The definition of  $T_{2\text{eff}}$  was chosen so that this expression would be true. This function is plotted in Fig. 4 for several different  $T_1$  values. For objects with  $T_1$  to  $T_2$  ratios of 10, which is typical for tissues at moderate to high field, the signal-to-noise ratio decreases only very slowly with asymptotic flip angle. This argues that low flip angle RARE may be very competitive with other acquisition methods.

Equation [11] has neglected the effect of the acquisition time on the time available for signal recovery prior to another excitation. Many of the applications for low flip angle RARE, including fast  $T_2$  and proton density imaging, require  $TR$  to be much longer than  $T_1$ . In these applications, the effect of the slightly longer acquisition on signal-to-noise ratio should be small but will depend on the  $TR$  selected for the application.

## METHODS

To experimentally verify the theory and evaluate the image quality, the low flip angle RARE sequence was

implemented on a clinical GE SIGNA 1.5 Tesla scanner equipped with a prototype gradient system. The gradient system could achieve gradient amplitudes of 23 mT/m and gradient switching speeds of 100  $\mu$ s. The strong and fast gradients made possible very compact echo trains. To further compress the echoes, a Hamming windowed 1.6 ms sinc pulse that was truncated at the first zero crossing was employed. With a 64 kHz acquisition bandwidth and a 256 frequency matrix, echo spacings of slightly under 5 ms were achievable.

Single-shot images were acquired by using ramp optimized RF pulse trains. An acquisition matrix of 256  $\times$  80, an FOV of 24  $\times$  15 cm, and a slice thickness of 5 mm were employed. To avoid artifacts in the reconstruction due to the higher amplitudes of the first two echoes, a total of 82 echoes were acquired and the first two were discarded. The phase encode ordering of Melki *et al.* (2) was used for all imaging. The acquisition of a single image required 410 ms.

To confirm the theoretical calculations, images of a uniform long  $T_2$  phantom were acquired with the phase encoding gradient turned off. The amplitude of each echo was then calculated. Such data were obtained for trains with asymptotic flip angles ranging from 180° to 17°. For comparison to the nonselective pulse theory, the amplitude of the slice select gradient for the refocusing pulses was reduced by a factor of four to achieve a more uniform flip angle across the slice. To avoid artifacts, the crusher gradients in the slice select direction were increased.

To assess the image quality, *in vivo* single-shot images were obtained in the brain of a normal volunteer. Flip angles from 90° to 17° were evaluated. At these flip angles, the images could be acquired with a  $TR$  of 500 ms without exceeding manufacturers safety limits on heating. Higher flip angles were not evaluated *in vivo*.

## RESULTS

Phantom measurements confirmed the validity of the theory. Echo amplitudes are plotted in Fig. 5 for several different asymptotic flip angles. The initial amplitudes of

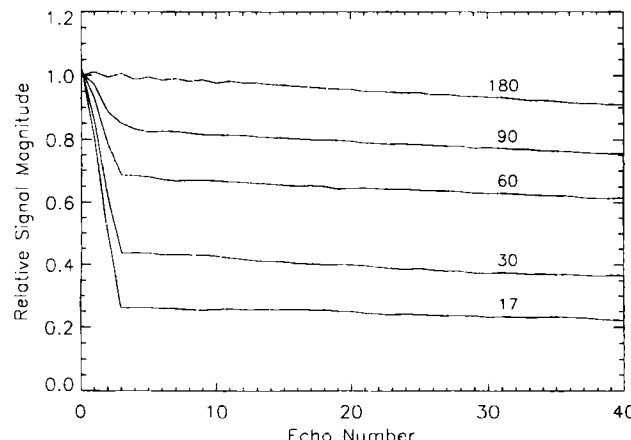


FIG. 5. Experimental echo amplitudes from a long  $T_2$  phantom using RF pulse trains optimized for a ramp down to a constant echo amplitude. Echo amplitudes from RF pulse trains with asymptotic flip angles of 180°, 90°, 60°, 30°, and 17° are plotted.

the echo trains are in excellent agreement with the theory. Also apparent in the figure is the excellent stability of echo amplitude that is possible with optimized RF pulse trains.

Axial single-shot images of the brain of a normal volunteer are shown in Fig. 6. The images demonstrate high signal-to-noise ratio and good spatial resolution. As expected, the image signal intensity for short  $TE$  images decreases with refocusing flip angle but signal-to-noise ratio is still fairly high with 30° refocusing pulses.  $T_2$ -weighted images are also shown, demonstrating the flexibility in selecting  $T_2$  contrast with the RARE sequence. Differences in the degree of  $T_2$  weighting are apparent in the images. This is best illustrated in Fig. 7 where  $T_{2\text{eff}}$  decay is shown for both 90° and 17° asymptotic refocusing flip angles. The short  $TE$  images were windowed for identical appearance but longer  $TE$  images show much more  $T_2$  weighting for the 90° flip angle than the 17° images. This is consistent with the increase in  $T_{2\text{eff}}$  expected in tissues with  $T_1$  much longer than  $T_2$ .

## DISCUSSION

A theory for the pseudosteady state signal amplitude in spin echo trains has been presented that provides a theoretical optimum signal intensity against which practical implementations can be compared. This theory sheds new light on the stability of CPMG (13, 15) echo trains and allows derivation of the asymptotic signal amplitude as a function of refocusing flip angle for such echo trains.

For the specific purpose of optimizing low flip angle RARE imaging, the theory has shown that constant amplitude low flip angle echo trains are inefficient at transferring signal intensity into the pseudosteady state condition. This inefficiency adds to the problems associated with the gradual approach of the echo amplitudes to the pseudosteady state. Flip angle optimized RF pulse trains are clearly superior both at producing a pseudosteady state rapidly and converting transverse magnetization into the pseudosteady state. RF pulse trains optimized for constant echo amplitude produce nearly the theoretical maximum signal amplitude at intermediate to high asymptotic flip angles but at lower asymptotic flip angles, the efficiency begins to drop. The efficiency at lower flip angles can be increased to nearly 100% by optimizing RF pulse trains for a downward ramp in echo amplitude from the 180° echo amplitude to the desired asymptotic echo amplitude. Experimental implementation of this approach (Fig. 5) confirmed the exceptionally high efficiency of these RF pulse trains. While this approach does improve sensitivity, it requires magnitude correction of the first few echoes prior to image reconstruction to avoid image artifact.

The use of low flip angles in the RF pulse train mixes both spin and stimulated echo components in the echo amplitudes. The decay rate of the echo amplitudes is thus determined by an effective  $T_2$ ,  $T_{2\text{eff}}$ , which is a mixture of  $T_1$  and  $T_2$ . For many tissues,  $T_1$  is much greater than  $T_2$ . In these tissues,  $T_{2\text{eff}}$  is longer than  $T_2$  but is still relatively insensitive to the value of  $T_1$ . For very low flip angle RF pulse trains or in tissues such as fat where  $T_1$  is not much longer than  $T_2$ ,  $T_1$  also has an

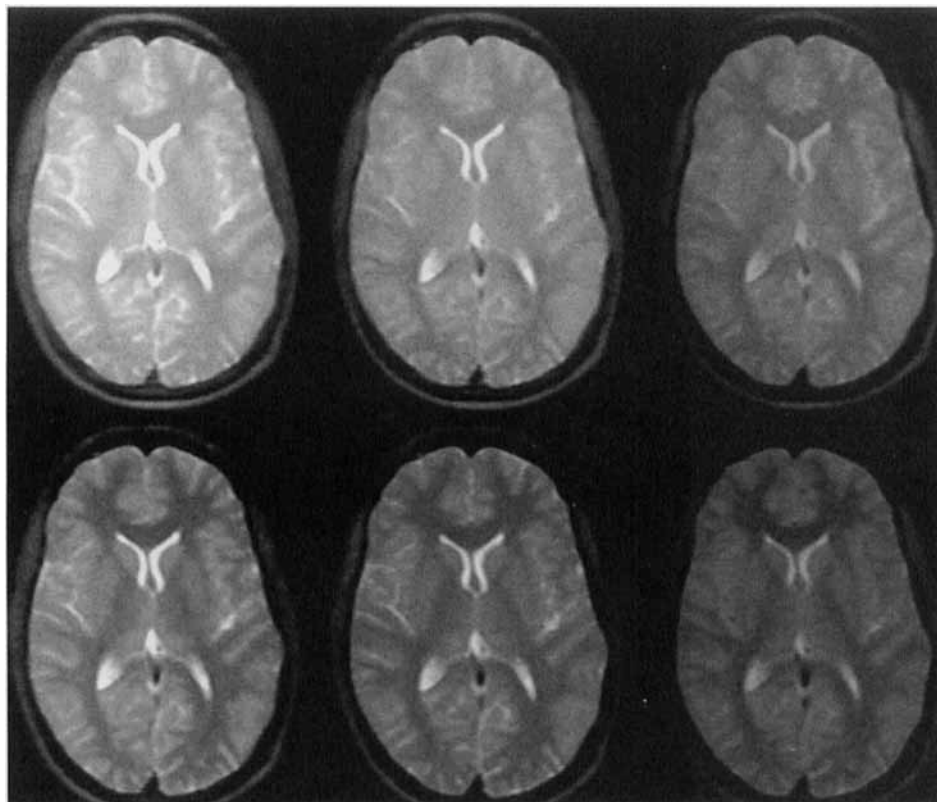


FIG. 6. Axial, single-shot RARE images through the brain of a normal volunteer. Images were obtained with ramp optimized RF pulse trains with asymptotic flip angles of 90° (left), 60° (center), and 30° (right). The images in the upper row were obtained with an effective  $TE$  of 18 ms, the lower row with an effective  $TE$  of 83 ms.

impact on contrast. In many pathologies,  $T_2$  and  $T_1$  change in the same direction. In such pathologies, the mixture of  $T_1$  and  $T_2$  decay should not strongly influence contrast, as long as a longer  $TE_{\text{eff}}$  is used to compensate for the longer  $T_{2\text{eff}}$ . In other pathologies, it is possible that  $T_{2\text{eff}}$  contrast will be poorer than  $T_2$  contrast.

Although the use of low refocusing flip angles does reduce the amplitude of the measured signal, the signal-to-noise ratio need not necessarily reduce proportionately. Accounting for the longer time available for imaging due to the longer  $T_{2\text{eff}}$  shows that the signal-to-noise ratio is nearly unchanged until asymptotic angles of under 60° are reached (Fig. 4). Practical applications of low flip angle RARE will have an even slower decrease in signal-to-noise ratio than in the figure because the analysis does not include the variation of data acquisition efficiency with bandwidth. For example, in the present implementation, a 64 kHz bandwidth was used that acquired a line of  $k$  space in 2 ms. The remaining 3 ms of the echo spacing were required for applying gradients and the pulse. At a lower flip angle where  $T_{2\text{eff}}$  is twice  $T_2$ , a 10-ms echo spacing could instead be used. Since the RF and gradient timing is unchanged, the entire additional 5 ms could be used for data acquisition by decreasing the bandwidth to 18 kHz. The practical reduction of noise is a factor of 1.9, rather than the 1.4 assumed in the theoretical considerations above, because the data acquisition efficiency increases from 40–70%.

Single-shot images in the brain of a normal volunteer demonstrate excellent image quality and the expected changes in signal amplitude and contrast with refocusing flip angle. Long echo-train imaging with reduced refocusing flip angles reduces the power deposition of the se-

quence dramatically. By employing 30° flip angles, for example, the signal amplitude is decreased by a factor of 2, the signal-to-noise ratio by 30%, yet the power deposition is reduced by a factor of 36 relative to a 180° train.

In practical application, and in the *in vivo* images shown in Figs. 6 and 7, slice selective refocusing pulses must be used and the imperfect slice profile will have implications for sensitivity and contrast. The methods of LeRoux and Hinks (10) for stabilizing the echo amplitudes when slice selective pulses are used can easily be applied to lower asymptotic flip angle RF pulse trains. As can be seen in Figs. 6 and 7, naive use of the nonselective pulse theory to tailor the amplitudes of selective pulses can produce images of excellent quality even though poorly selective pulses were used. Accurately accounting for the effects of slice selection will likely slightly alter the optimized RF pulse amplitudes and slightly increase the  $T_{2\text{eff}}$  relative to the nonselective pulse theory. Since the RF power in low flip angle RARE is lower than when 180° pulses are used, RF pulses with better slice profiles but that deposit more RF power might be employed. This would lead to more uniformity of contrast across the slice.

The variation of RF amplitude, which typically occurs within a practical RF coil, has been neglected in this work. Experience with the standard head coil, in which the amplitude variations are of the order of 10%, and with the body coil, in which amplitude variation can be considerably higher than the head coil, suggests that RF inhomogeneity is not a major problem for this method. Errors in the amplitude of the RF pulse train will cause slight amplitude fluctuations in the first few echoes. These fluctuations could produce subtle artifacts, espe-

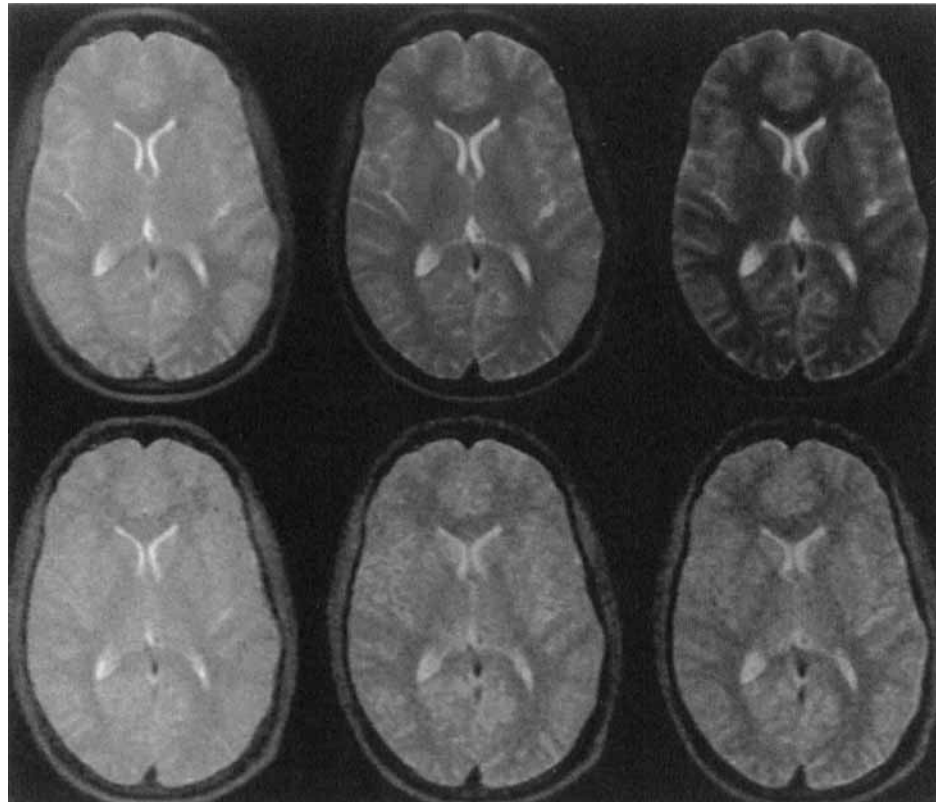


FIG. 7. Comparison of apparent  $T_2$  decay in images obtained using ramp optimized RF pulse trains with asymptotic flip angles of  $90^\circ$  (top), and  $17^\circ$  (bottom). The difference of  $T_2$  decay in the images obtained at  $TE$ 's of 18 ms (left), 83 ms (center), and 157 ms (right) is clearly apparent.

cially in proton density images where the center of  $k$ -space is scanned in the first echoes. Discarding the first few echoes may be sufficient to eliminate these artifacts. Contrast will also be slightly affected by RF inhomogeneity because  $T_{2\text{eff}}$  will be longer when the RF amplitude is weaker.

The major disadvantage of long echo-train imaging is the increased acquisition time required for each slice. This reduces the number of slices that can be acquired in a given repetition time and can lead to inefficiency in data acquisition. In this respect, long echo-train RARE imaging is similar to fast gradient-echo imaging. Long echo-train RARE imaging will most likely be optimal in applications where fast or motion insensitive imaging is required or in 3-dimensional sequences. The extension of the number of echoes made possible by low flip angle RF pulse trains may make it possible to acquire 3-dimensional  $T_2$  images without the use of multiple slab acquisitions (16) that can suffer from slab boundary artifacts. Reduced flip angle echo trains need not be limited to long echo train acquisitions. In multiple slice interleaved RARE acquisitions at high field, power deposition can restrict the number of slices that can be acquired. In such circumstances, reduced flip angles can be used, although the signal-to-noise ratio will decrease more like the echo amplitude plotted in Fig. 1 rather than the signal-to-noise ratio plotted in Fig. 4 because the extended acquisition time available in each slice was not used for data acquisition.

The single-shot images in Figs. 6 and 7 invite comparison with other single shot techniques including echo planar (17), GRASE (18), and prepared gradient echo sequences (19). Single-shot RARE does not suffer from

the distortion and ghosting artifacts that plague echo-planar imaging so it may be competitive with echo-planar imaging for motion insensitive  $T_2$  and proton density imaging. However, echo-planar imaging can be operated in low flip angle gradient echo mode, allowing for higher temporal resolution than is feasible with RARE, and echo planar acquisitions are generally a factor of 2 to 4 times faster than RARE acquisitions. Because the CPMG condition is required, the RARE acquisition is also harder to prepare with contrasts such as  $T_2^*$  and diffusion, although approaches to overcoming these problems have been discussed (7). Low flip angle RARE is directly compatible with the acquisition of multiple gradient echoes per echo train as are used in GRASE. Optimized RF pulse trains have previously been suggested as an approach to reduce the  $T_2$  decay artifacts in GRASE (20). As discussed earlier, the use of low refocusing flip angles in RARE does make possible data acquisition efficiencies of 70%, which are comparable with those of GRASE (21), with the better point spread function of RARE (22).

The existence of a pseudosteady state and the use of low flip angle RF pulse trains in a RARE sequence seem to blur the distinction between fast gradient-echo and RARE imaging. In truth, there is little difference between RARE and prepared gradient echo sequences where the signal due to  $T_1$  recovery during the acquisition is crushed by applied gradients (23) except that the theory for RARE explicitly takes into account the multiple spin and stimulated echoes that can occur in such sequences. There is a major difference between RARE and equilibrium fast gradient echo sequences, however, because  $T_1$  recovery of magnetization plays a major role in such gradient echo sequences. For long echo train, low flip

angle RARE sequences, a fast gradient echo signal appropriate for the flip angle does begin to appear, but it is attenuated by the lack of slice refocusing, frequency prephasing, and additional crusher gradients.

In summary, the use of a refocusing flip angle other than 180° in RARE sequences can be advantageous for reasons of imaging speed and power deposition without severely affecting signal-to-noise ratio or contrast. The refocusing flip angle represents yet another parameter that should be investigated in optimizing imaging applications.

## APPENDIX

### Derivation of the Pseudosteady State Solution

To derive Eqs. [4] and [5] from Eq. [3], first solve the third component of Eq. [3] for  $M_z$ .

$$M_z = \frac{\sin\alpha \exp i\left(\beta + \frac{\phi}{2}\right)}{2(1 - \cos\alpha)} M_t + \frac{\sin\alpha \exp -i\left(\beta + \frac{\phi}{2}\right)}{2(1 - \cos\alpha)} M^* t \quad [A1]$$

Substituting for  $M_z$  in the top component of Eq. [3] yields

$$\begin{aligned} M_t & \left[ 1 - \cos^2 \frac{\alpha}{2} \exp i(\beta + \delta + \phi) + \frac{\sin^2 \alpha \exp i(\beta + \delta + \phi)}{2(1 - \cos\alpha)} \right] \\ & = \left[ -\sin^2 \frac{\alpha}{2} \exp -i(\beta - \delta) - \frac{\sin^2 \alpha \exp -i(\beta - \delta)}{2(1 - \cos\alpha)} \right] M^* t \end{aligned} \quad [A2]$$

Multiplying by  $(1 - \cos\alpha)$  and substituting the trigonometric relations,

$$\cos^2 \frac{\alpha}{2} = \frac{(1 + \cos\alpha)}{2} \quad \sin^2 \frac{\alpha}{2} = \frac{(1 - \cos\alpha)}{2} \quad [A3]$$

yields

$$\begin{aligned} M_t & \left[ (1 - \cos\alpha) - \frac{(1 + \cos\alpha)(1 - \cos\alpha)}{2} \exp i(\beta + \delta + \phi) \right. \\ & + \frac{\sin^2 \alpha \exp i(\beta + \delta + \phi)}{2} \left. \right] = \left[ -\frac{(1 - \cos\alpha)^2}{2} \exp -i(\beta - \delta) \right. \\ & \left. - \frac{\sin^2 \alpha \exp -i(\beta - \delta)}{2} \right] M^* t \end{aligned} \quad [A4]$$

which simplifies to

$$M^* t = -\exp i(\beta - \delta) M_t \quad [A5]$$

This can be substituted back into the expression for  $M_z$  to yield

$$M_z = \frac{i \sin\alpha \exp i\left(\frac{\beta - \delta}{2}\right) \sin\left(\frac{\beta + \delta + \phi}{2}\right)}{(1 - \cos\alpha)} M_t \quad [A6]$$

If it is assumed that all of the equilibrium magnetization,  $M_0$ , has been transferred to the pseudosteady state then

$$M_0^2 = |M_t|^2 + |M_z|^2 = \left( 1 + \left( \frac{\sin\alpha \sin\left(\frac{\beta + \delta + \phi}{2}\right)}{1 - \cos\alpha} \right)^2 \right) |M_t|^2 \quad [A7]$$

Since Eq. [A5] determines the complex conjugate of  $M_t$ , Eq. [A7] can be solved for  $M_t$ ,

$$M_t = \pm i M_0 \exp -i\left(\frac{\beta - \delta}{2}\right)$$

$$\cdot \left( 1 + \left( \frac{\sin\alpha \sin\left(\frac{\beta + \delta + \phi}{2}\right)}{1 - \cos\alpha} \right)^2 \right)^{-\frac{1}{2}} \quad [A8]$$

The amplitude of the resulting echo is given by averaging over all  $\phi$ .

$$\begin{aligned} M_{\text{echo}} & = i \frac{M_0 \exp -i\left(\frac{\beta - \delta}{2}\right)}{2\pi} \int_0^{2\pi} d\phi \\ & \cdot \left( 1 + \left( \frac{\sin\alpha \sin\left(\frac{\beta + \delta + \phi}{2}\right)}{1 - \cos\alpha} \right)^2 \right)^{-\frac{1}{2}} \end{aligned} \quad [A9]$$

Using the relationship

$$\sin^2 \left( \frac{\beta + \delta + \phi}{2} \right) = \frac{(1 - \cos(\beta + \delta + \phi))}{2} \quad [A10]$$

and shifting the limits of integration to eliminate  $\beta$  and  $\delta$ , Eq. [A9] can be rewritten as

$$\begin{aligned} M_{\text{echo}} & = i \frac{M_0 \exp -i\left(\frac{\beta - \delta}{2}\right)}{2\pi} \int_0^{2\pi} d\phi \left( 1 + \frac{1}{2} \left( \frac{\sin\alpha}{1 - \cos\alpha} \right)^2 \right. \\ & \left. - \frac{1}{2} \left( \frac{\sin\alpha}{1 - \cos\alpha} \right)^2 \cos\phi \right)^{-\frac{1}{2}} \end{aligned} \quad [A11]$$

The following formula, Gradshteyn and Ryzhik (14), Eq. [3.661.3]

$$\frac{1}{2\pi} \int_0^{2\pi} dx (a + b \cos x)^n = (a^2 - b^2)^{\frac{n}{2}} P_n \left( \frac{a}{(a^2 - b^2)^{\frac{1}{2}}} \right) \quad [A12]$$

can be used to solve the integral. The result is

$$M_{\text{echo}} = i M_0 \exp -i \left( \frac{\beta - \delta}{2} \right)$$

$$\left( 1 + \left( \frac{\sin \alpha}{(1 - \cos \alpha)} \right)^2 \right)^{-\frac{1}{4}} P_{-\frac{1}{2}} \left( \frac{\left( 1 + \frac{1}{2} \left( \frac{\sin \alpha}{(1 - \cos \alpha)} \right)^2 \right)^{\frac{1}{2}}}{1 + \left( \frac{\sin \alpha}{(1 - \cos \alpha)} \right)^{\frac{1}{2}}} \right) \quad [\text{A13}]$$

Using the relationship

$$1 + \left( \frac{\sin \alpha}{(1 - \cos \alpha)} \right)^2 = \frac{(1 - \cos \alpha)^2 + \sin^2 \alpha}{(1 - \cos \alpha)^2}$$

$$= \frac{1 - 2 \cos \alpha + \cos^2 \alpha + \sin^2 \alpha}{(1 - \cos \alpha)^2} \quad [\text{A14}]$$

$$= \frac{2 - 2 \cos \alpha}{(1 - \cos \alpha)^2} = \frac{2}{(1 - \cos \alpha)} = \left( \sin^2 \frac{\alpha}{2} \right)^{-1}$$

Eq. [A13] can be rewritten as

$$M_{\text{echo}} = i M_0 \exp -i \left( \frac{\beta - \delta}{2} \right)$$

$$\left( \sin \frac{\alpha}{2} \right)^{\frac{1}{2}} P_{-\frac{1}{2}} \left( \sin \frac{\alpha}{2} \left( 1 + \frac{1}{2} \left( \frac{\sin \alpha}{(1 - \cos \alpha)} \right)^2 \right) \right) \quad [\text{A15}]$$

$$= i M_0 \exp -i \left( \frac{\beta - \delta}{2} \right) \left( \sin \frac{\alpha}{2} \right)^{\frac{1}{2}} P_{-\frac{1}{2}} \left( \sin \frac{\alpha}{2} \left( 1 + \frac{1}{8} \frac{\sin^2 \alpha}{\sin^4 \frac{\alpha}{2}} \right) \right)$$

## REFERENCES

1. J. Hennig, A. Nauerth, H. Friedburg, RARE imaging: a fast imaging method for clinical MR. *Magn. Reson. Med.* **3**, 823–833 (1986).
2. P. S. Melki, R. V. Mulkern, L. P. Panych, F. A. Jolesz, Comparing the FAISE Method with Conventional Dual-Echo Sequences. *J. Magn. Reson. Imaging* **1**, 319–326 (1991).
3. P. S. Melki, F. A. Jolesz, R. V. Mulkern, Partial RF echo-planar

imaging with the FAISE method. II. Contrast equivalence with spin-echo sequences. *Magn. Reson. Med.* **26**, 342–354 (1992).

4. J. N. Rydberg, C. A. Hammond, R. C. Grimm, B. J. Erickson, C. R. Jack, J. Huston, S. J. Riederer, Initial clinical experience in MR imaging of the brain with a fast fluid-attenuated inversion recovery pulse sequence. *Radiology* **193**, 173–180 (1994).
5. G. Reuther, B. Kiefer, A. Tuchmann, Cholangiography before biliary surgery: single-shot MR cholangiography versus intravenous cholangiography. *Radiology* **198**, 561–6 (1996).
6. P. S. Melki, R. V. Mulkern, magnetization transfer effects in multislice RARE sequences. *Magn. Reson. Med.* **24**, 189–195 (1992).
7. D. G. Norris, P. Bornert, T. Reese, D. Leibfritz, On the Application of ultra-fast RARE experiments. *Magn. Reson. Med.* **27**, 142–164 (1992).
8. P. S. Melki, F. A. Jolesz, R. V. Mulkern, Partial RF echo planar imaging with the FAISE method. I. Experimental and theoretical assessment of artifact. *Magn. Reson. Med.* **26**, 328–341 (1992).
9. J. Hennig, Multiecho imaging sequences with low refocusing flip angles. *J. Magn. Reson.* **78**, 397–407 (1988).
10. P. LeRoux, R. S. Hinks, Stabilization of echo amplitudes in FSE sequences. *Magn. Reson. Med.* **30**, 183–191 (1993).
11. R. R. Ernst, W. A. Anderson, Application of Fourier transform spectroscopy to magnetic resonance. *Rev. Sci. Instrum.* **37**, 93–192 (1966).
12. E. T. Jaynes, Matrix treatment of nuclear induction. *Phys. Rev.* **98**, 1099–1105 (1955).
13. S. Meiboom, D. Gill, Modified spin-echo method for measuring nuclear relaxation times. *Rev. Sci. Instrum.* **29**, 668–691 (1958).
14. I. S. Gradshteyn, I. M. Ryzhik, "Table of Integrals, Series, and Products." Academic Press, San Diego, 1994.
15. H. Y. Carr, E. M. Purcell, Effects of diffusion on free precession in nuclear magnetic resonance experiments. *Phys. Rev.* **94**, 630–638 (1954).
16. K. Oshio, F. A. Jolesz, P. S. Melki, R. V. Mulkern,  $T_2$ -weighted thin-section imaging with the multislab three-dimensional RARE technique. *J. Magn. Reson. Imaging* **1**, 695–700 (1991).
17. P. Mansfield, I. L. Pykett, Biological and medical imaging by NMR. *J. Magn. Reson.* **29**, 355 (1978).
18. K. Oshio, D. A. Feinberg, GRASE (gradient- and spin-echo) imaging: a novel fast MRI technique. *Magn. Reson. Med.* **20**, 344–349 (1991).
19. A. Haase, Snapshot FLASH MRI: applications to  $T_1$ ,  $T_2$ , and chemical-shift imaging. *Magn. Reson. Med.* **13**, 77–89 (1990).
20. T. Schaffter, P. Bornert, D. Leibfritz, PSF improvements in single shot GRASE imaging, in "Proc., SMR 2nd Annual Meeting, San Francisco, 1994," p. 27.
21. D. A. Feinberg, B. Kiefer, G. Johnson, GRASE improves spatial resolution in single shot imaging. *Magn. Reson. Med.* **33**, 529–533 (1995).
22. D. A. Feinberg, G. Johnson, B. Kiefer, Increased flexibility in GRASE imaging by k space-banded encoding. *Magn. Reson. Med.* **34**, 149–155 (1995).
23. K. D. Merboldt, W. Hanicke, H. Bruhn, M. L. Gyngell, J. Frahm, Diffusion imaging of the human brain in vivo using high speed STEAM MRI. *Magn. Reson. Med.* **23**, 179–192 (1992).